

D. Aleinikava and A.B. Kuklov

Interplay of non-linear elasticity and dislocation-induced superfluidity in solid ^4He

10.27.2011

Keywords Supersolid, shear modulus, dislocations, superfluidity

Abstract The mechanism of the roughening induced partial depinning of gliding dislocations from ^3He impurities is proposed as an alternative to the standard "boiling off". We give a strong argument that ^3He remains bound to dislocations even at large temperatures due to very long equilibration times. A scenario leading to the similarity between elastic and superfluid responses of solid ^4He is also discussed. Its main ingredient is a strong suppression of the superfluidity along dislocation cores by dislocation kinks (D. Aleinikava, et. al., arXiv:0812.0983). These kinks, on one hand, determine the temperature and ^3He dependencies of the generalized shear modulus and, on the other, control the superfluid response. Several proposals for theoretical and experimental studies of solid ^4He are suggested.

PACS numbers:

1 Introduction

The discovery of the torsional oscillator (TO) anomaly by Kim & Chan in 2004¹, which was originally ascribed to the non-classical moment of inertia (NCRI)², has reignited a strong interest to the supersolidity³ in solid ^4He . However, after observing the enigmatic similarities between the TO and the shear modulus by Day & Beamish⁴ (the similar effect has been observed by Tsymbalenko⁵ at significantly higher temperatures and frequencies), serious doubts have been raised⁶ about the supersolid interpretation of the TO anomaly. Very recently in Ref.⁷ it has

Department of Engineering Science and Physics, CSI, CUNY,
Staten Island, NY 10314, USA
Tel.: 1-718-982-2887
Fax: 1-718-982-2830
E-mail: Anatoly.Kuklov@csi.cuny.edu

been shown that the deformation of solid ^4He in the torsion rod is fully responsible for the anomaly reported by several groups.

A completely different approach has been undertaken by Ray & Hallock⁸ who have observed the direct superflow through solid ^4He at very small rate – about 3g/year. Thus, it is very likely that such a signal is below the sensitivity of the TO⁸. Under these circumstances, it is natural to ask: is there any "room" left for observing the supersolidity in the TO-approach?

While not providing a definite answer to this question, we show that the superfluid (SF) response of the dislocation cores (found to be SF in the *ab initio* simulations^{9,10}) can mimic the temperature and ^3He dependencies of the generalized shear modulus⁴ (see Eq.(22)). The key to such a similarity is a possibility that dislocation kinks strongly suppress the superfluidity along the core¹¹ (cf. also a proposal by Balibar¹²).

Our paper is organized as follows: in Sec.2 the shear modulus anomaly⁴ is discussed in terms of the dislocation roughening in the presence of the Peierls and ^3He pinning potentials. The inconsistency of the ^3He "boiling off" scenario is revealed, and it is suggested that ^3He remains bound to dislocations even at high T . The puzzle of the "missing dissipation" is addressed in Sec.3. Then, in Sec.4 we will discuss the coarse grained model where the SF order parameter interacts with the thermal kinks, and will show that the condensate fraction can resemble the shear modulus T - and the ^3He - dependencies. We also discuss a mechanism linking the dissipation in the SF and in the gliding dislocation subsystems to the common bath of thermal kinks. Finally, in Sec.5 we give a brief summary of the results and outline proposals for future studies.

2 Generalized shear modulus

The shear modulus anomaly of many materials is caused by liberation of gliding dislocations from the low temperature pinning by either impurities^{13,4} or by the Peierls potential^{11,14}. As shown in Ref.¹⁵, the reconciling of the observed T -dependencies of the shear modulus $G(T)$ with the "boiling off"-model of ^3He impurities from the dislocation cores requires introducing a wide distribution of ^3He activation energies E_a – as wide as the mean energy itself. The origin of such a wide distribution in a crystal with relatively low dislocation densities (about $x_d \approx 10^{-7} - 10^{-8}$ in the atomic units of the typical distance between ^4He atoms $b \approx 3.5 - 3.7\text{\AA}$) is very puzzling and raises more questions than gives answers.

In this section we argue that the actual shape of $G(T)$ in the presence of the Peierls potential and the ^3He pinning is determined by thermal roughening of gliding dislocations: thermal and quantum fluctuations of dislocation shape wash out both potentials. This process is the alternative to the "boiling off" mechanism.

2.1 Fluctuative depinning of gliding dislocation

In solid ^4He dislocations are strongly pinned by the Frank's forest cross-linking points¹³ and, in addition, are weakly pinned by Peierls potential and ^3He impurities. The model capturing both effects relies on the Granato-Lücke-type string¹⁶

description^{11,14} subjected to both the Peierls potential U_P and the trapping potential U_t provided by ^3He atom. The corresponding action capturing quantum and thermal effects can be written in the imaginary time τ as

$$H = \int_0^L dx \int_0^\beta d\tau \left(\frac{1}{2K} ((\nabla_x y)^2 + (\nabla_\tau y)^2) - \sigma y - U_P(y) - N(x)U_t(y) \right), \quad (1)$$

$$U_P(y) = -\alpha \cos(2\pi y), \quad U_t(y) = N(x)V(y), \quad V(y) = -V_0 \exp(-(y/y_0)^2), \quad (2)$$

where $y(x, \tau)$ is the dislocation displacement from its equilibrium position in a gliding plane; L stands for the dislocation length between the cross-linking points ($y(x=0, \tau) = y(x=L, \tau) = 0$); $\beta = 1/T$ (in atomic units $\hbar = 1, K_B = 1$); K denotes the Luttinger parameter¹⁴; σ denotes external stress; α, V_0 stand for the strength of the Peierls and the trapping potentials, respectively; $N(x)$ gives the density of ^3He impurities which can be located at any point $0 < x < L$ along the line $y = 0$; the trapping potential is chosen as a Gaussian with some range $y_0 \sim 1$.

In Eqs.(1,2) and below all lengths are measured in units of Burger's vector b , and the unit of time is chosen so that the speed of sound V_s along the core is unity. Accordingly, the unit of energy (temperature) is given by $T_o = \hbar V_s / K_B b = 1$ (which is $\sim 10\text{K}$ in standard units). All our results below are represented in such dimensionless units.

The parameters can, in principle, be extracted from the *ab initio* simulations. For example, Ref.¹⁷ provides the estimate $V_0 \approx 0.8\text{K}$ for binding of ^3He to screw dislocation. In our simplified model we ignore the long-range part of the trapping potential, which should scale as $V(y) \sim -1/|y|$ for the case of edge dislocation (and as $\sim -1/y^2$ for the screw dislocation¹⁷).

In Ref.¹⁸ it has been suggested that ^3He atoms don't actually provide pinning for dislocations, and, instead, they induce a viscous drag force. Here we take a different approach: due to the extremely narrow band width $J \sim 10^{-4}\text{K}$ ¹⁹, a ^3He atom-impuriton, once bound to a dislocation, can be easily localized in the lattice potential to become an immobile pinning center.

Monte Carlo simulations of the partition function $Z = \int Dy \exp(-H)$ as well as any needed mean $\langle \dots \rangle = \int Dy \dots \exp(-H) / Z$ have been conducted in discretized space-time lattice using the gradient expansion method combined with the Worm Algorithm²⁰ with the ^3He impurities considered as Boltzmann particles of fixed total number, with $N(x) = 0, 1$ depending on if ^3He atom is or is not present along a given space-time line (x, τ) , respectively. This model is similar to the one considered in Ref.¹⁴ where $V_0 = 0$. Here we ignore the long-range potential between kinks¹⁴.

The response of the model (1) can be related to the average coarse-grained shear modulus¹⁴. If $y(x, t)$ is a typical dislocation displacement of an element of Frank's forest of typical sizes L, L_y, L_z (along the respective axes x, y, z), the average strain is $\approx \int y(x, t) dx / (LL_y L_z)$ (in the chosen units). Since $y \propto \sigma$, and the total strain must include the elastic one σ / G_{el} , with G_{el} being bare shear modulus, the resulting (inverse) shear modulus for static σ becomes $G^{-1} = G_{el}^{-1} + \Lambda \langle y \rangle / (LL_y L_z \sigma)$, where Λ is some orientation averaging factor¹⁶ ~ 1 . In the limit $\sigma \rightarrow 0$ this gives

$$\frac{1}{G} = \frac{1}{G_{el}} + \frac{n_d \Lambda}{L} \int_0^\beta d\tau \int_0^L dx \int_0^L dx' \langle y(x', \tau) y(x, 0) \rangle \quad (3)$$

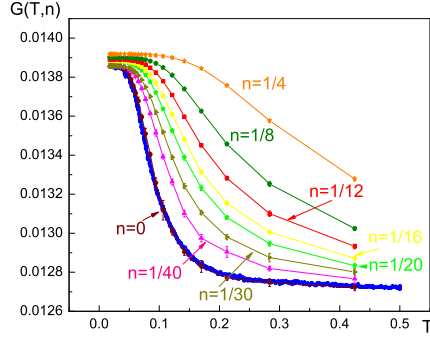


Fig. 1 (Color online) Shear modulus G from Ref.⁴ for 1 ppb of ^3He at $f = 2000\text{Hz}$ (blue dots) and the MC results (1,3) for various (linear) concentrations n of ^3He impurities.

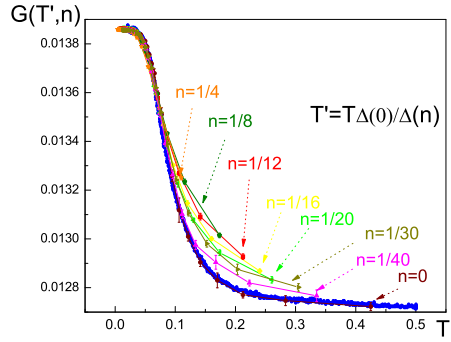


Fig. 2 (Color online) The experimental data⁴ are the same as in Fig. 1. The family of the MC curves from Fig. 1 has been collapsed to a single master curve by rescaling the T -axis and slightly adjusting G_{el} to allow all curves to have the common value at $T = 0$. The simulation parameters are chosen as $K = 0.1, V_0 = 0.3, y_0^{-1} = 4.2$ and the Peierls potential amplitude $\alpha = 0.01$ (in units of T_o, b) was adjusted to achieve best agreement with the experiment at $n = 0$.

where $n_d = 1/(L_y L_z) \approx 1/L^2 \ll 1$ stands for density of dislocations in the units of b and the mean $\langle \dots \rangle$ is evaluated with respect to the action (1) at $\sigma = 0$.

The results of the simulations are presented in Figs. 1,2 for the case of pure Peierls potential ($n = 0$, cf.¹⁴) as well as for a set of finite linear densities n of ^3He . For larger n the softening of $G(T, n)$ occurs at larger T . Such tendency is clearly seen in Fig.1. We have found that the curves for different n are almost self-similar to each other and can be collapsed to a single master curve, Fig. 2, by choosing a proper multiplicative factor $T_\Delta: T \rightarrow T_\Delta T$. The simulations have been conducted for fixed values of n , that is, ^3He atoms were not allowed to boil off from the dislocation. Despite that and the strong pinning at the dislocation ends,

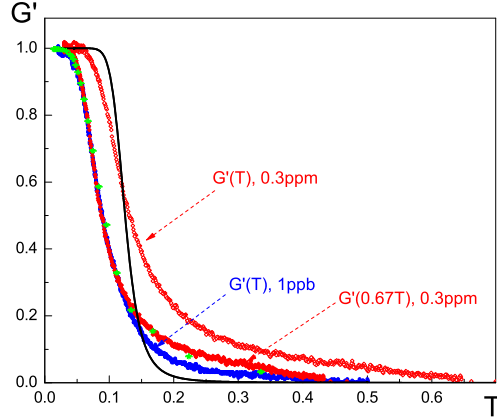


Fig. 3 (Color online) The shear modulus ($f = 2000\text{Hz}$) normalized by its maximum variation for two different ${}^3\text{He}$ concentrations 1 ppb (blue dots) and 0.3ppm (open red rhombi)⁴. The data for 0.3ppm is also shown for the rescaled temperature $T \rightarrow 0.67T$ (filled rhombi). The Monte Carlo data (stars) for $n = 1/40$ of ${}^3\text{He}$ from Fig. 1 is shown at the same rescaled temperature. Black solid line: the attempt to fit the 0.3ppm data by the "boiling off" model with the parameters chosen $n_d = 0.3 \cdot 10^{-8}$, $E_a = 0.65\text{K}$.

thermal kinks induce fluctuations of the dislocation position y around $y = 0$ so that the Peierls and the ${}^3\text{He}$ -pinning potentials are essentially washed out, and the modulus can reach its high- T value.

The rescaling parameter T_Δ reflects the value of the dislocation gap $\Delta = T_\Delta^{-1}$ induced by the pinning potentials. We have found that Δ grows with n . This can be understood from the following consideration: at small n the effect of impurities is inducing some effective average potential $\sim -nV_0 \exp(-(y/y_0)^2) \approx -nV_0(1 - (y/y_0)^2)$ in the action (1). This corresponds to the formation of the effective gap $\sim \Delta \approx \sqrt{nV_0}/y_0$. As n grows, the effect of the impurity-impurity repulsion through the string excitations becomes important (the pinning increases the zero-point energy of the dislocation phonons and kinks). Thus, the gap must show a crossover from $\Delta \sim \sqrt{\Delta_0^2 + \dots n}$ at small n to $\Delta \sim n$ at large n , where $\Delta_0^2 \sim \alpha$ is attributed to the Peierls potential. The fit by such quadratic function gives $\Delta(n) = \sqrt{\Delta^2(0) + \delta_1 n + \delta_2 n^2}$, $\Delta(0) = 0.209 \pm 0.005$, $\delta_1 = 1.17 \pm 0.06$, $\delta_2 = 5.3 \pm 0.3$.

It is important that, while strongly fluctuating dislocation becomes practically free from the pinning potentials, it still provides a very strong binding potential \tilde{V}_0 to the impurities on average if compared to the impuriton band-width J . Indeed, we estimate \tilde{V}_0 as $V(y)$, Eq.(2), smeared by large fluctuations of the dislocation position y around $y = 0$ as

$$\tilde{V}_0 \approx \frac{y_0}{\sqrt{\langle y^2 \rangle}} V_0 = y_0 \sqrt{\frac{T_D}{TL}} V_0 \ll V_0, \quad (4)$$

where the thermal fluctuations are taken in the high- T limit as $\langle y^2 \rangle \approx TL/T_D > y_0^2$ and T_D stands for Debye temperature. An estimate of \tilde{V}_0/J for the typical values ($V_0 \sim 1\text{K}, T \sim 1\text{K}, T_D \sim 10\text{K}, y_0 \sim 1, L \sim 1/\sqrt{n_d} \sim 10^4 - 10^5$) shows that $\tilde{V}_0/J \sim 10^2$. As discussed below in Sec.2.2, such large ratio implies very long equilibration time for ^3He to boil off into bulk.

2.2 Fluctuative partial depinning versus boiling off of ^3He

Figs. 1,2 represent the result of the fluctuative creep—quantum and thermal fluctuations of the dislocation shape due to kinks and phonons produce decoupling of the dislocation line from the Peierls and ^3He -pinning potentials. In other words, despite the presence of impurities at the equilibrium dislocation position $\langle y \rangle = 0$, the spatially averaged pinning force acting on the dislocation is significantly diminished by the shape fluctuations. The question is how allowing ^3He to boil off will modify the curves $G(T, n)$.

Let's, first, turn attention to the experimental situation. Fig. 3 shows Day & Beamish data for $G(T)$ at two vastly different bulk concentrations of ^3He . These moduli can be collapsed on each other and fit by the Monte Carlo data obtained under the assumption that ^3He does not boil off. In contrast, the boiling off model with the single activation energy can fit neither of $G(T)$ (cf.¹⁵). In other words, the experiment indicates that ^3He remains bound to the dislocation even at high temperatures, which is consistent with the conjecture of very long thermalization time (as our estimates indicate — much longer than any reasonable experimental time) of the impuritons.

The equilibrium concentration $n(T)$ of ^3He on dislocations at density n_d can be found within the simplest thermodynamics consideration treating ^3He atoms as non-interacting Boltzmann particles²¹:

$$n(T) = \frac{X_3}{n_d + \exp(-E_a/T)}, \quad (5)$$

where we assume the total (bulk) fraction X_3 of ^3He as $X_3 \leq n_d$ (in the chosen units) and E_a stands for ^3He activation energy. This equation is also valid for $X_3 > n_d$ as long as $T > E_a/|\ln(X_3 - n_d)|$.

The boiling off starts at $T_{\text{bon}} \approx E_a/|\ln(n_d)| \ll E_a$ for the realistic densities of dislocations $n_d \sim 10^{-6} - 10^{-9}$. Given the typically accepted $E_a \sim 0.5 - 0.8\text{K}$, this gives the boiling off onset temperature as $T_{\text{bon}} \sim 40 - 70\text{mK}$. The pinning becomes irrelevant when the typical distance $r \sim 1/n$ between the trapped atoms is larger than $L \approx 1/\sqrt{n_d}$, Ref.⁴. This determines the upper temperature T_{bup} when all ^3He atoms have essentially evaporated as $T_{\text{bup}} \approx E_a/|\ln(X_3/\sqrt{n_d})|$. For the standard values of $X_3 \sim 10^{-6} - 10^{-9} \ll 1$ this gives $T_{\text{bup}} \approx 70 - 100\text{mK}$ implying that the actual softening range should be much narrower ($\leq 30\text{mK}$) (see the solid black line in Fig. 3) than it is observed experimentally⁴.

The pure boiling off model corresponds to the action (1) without Peierls potential ($\alpha = 0$). In the approximation of strong pinning ($V_0 \rightarrow \infty$) by the impurities placed (equidistantly a distance $r = 1/n(T)$, Eq.(5), apart from each other) along

the dislocation of the length $L \approx 1/\sqrt{n_d}$ one finds (using the free string solution¹⁶ between two pinning centers) the shear modulus (3)

$$\frac{1}{G(T)} = \frac{1}{G_{el}} + \frac{\gamma}{1+n^2/n_d}, \quad \gamma \equiv \frac{1}{G(\infty)} - \frac{1}{G_{el}}. \quad (6)$$

This equation together with Eq.(5) have been used to obtain the solid fitting curve in Fig. 3 for the parameters typical for solid ⁴He. As can be seen, this fit is not adequate²².

Similarly, the attempt to include the boiling off mechanism into the Monte Carlo data by replacing n by the form (5) leads to the same failure if one chooses the realistic values of n_d, E_a, X_3 . Simply saying, if the equilibrium were reached fast on the experimental scale, there would be no impurities left on dislocations to affect the curve $G(T)$ at $T \geq 0.07 - 0.1\text{K}$. Nevertheless, as discussed above, the fluctuative mechanism completely ignoring the evaporation of ³He from dislocations can describe well the temperature dependence of $G(T)$ in a wide range of ³He concentrations. In other words, it appears that the actual equilibrium between binding to dislocations and being free in the bulk cannot be established for ³He atoms in any reasonable experimental time. Accordingly, the amount of ³He trapped by a dislocation is predetermined during crystal growth.

The following considerations may help to understand our conjecture: ³He atoms in a solid ⁴He exist as impuritons with a very narrow band-width J so that any repulsive or attractive potential characterized by energies larger than J causes a ³He atom to be localized within a spatial region of a size on which the potential energy changes by not more than J , Ref.¹⁹. Furthermore, bulk phonons which are responsible for establishing the equilibrium can only change an impuriton energy by J which is much smaller than \tilde{V}_0 , Eq.(4). In other words, there is no chance for an impuriton to be freed into the bulk by just absorbing the necessary thermal energy during one scattering event. Instead, it must diffuse through the energy landscape with the help of many scattering events $\sim (\tilde{V}_0/J)^2 \gg 1$. Since the corresponding scattering matrix elements are suppressed as high powers of T/T_D and J/T_D , Ref.¹⁹, such diffusion must be strongly suppressed. The detailed solution of this problem along the line of the approach²³ will be presented elsewhere.

The inconsistency of the boiling off mechanism has already been noted in Ref.¹⁵. Here we have shown that the alternative scenario is the fluctuative partial depinning of dislocation from the Peierls and ³He pinning potentials. Within this scenario the corresponding activation energy seen experimentally^{24,25,15} should be attributed to the kink-pair creation energy (dependent on strengths of the both potentials) rather than to the activation of ³He from a stationary dislocation.

3 The puzzle of "missing dissipation"

Both phenomena—the NCRI and the shear anomalies—are characterized by the dissipation peak in the region of fast variation of $G(T)$ and the NCRI fraction $\rho_s(T)$. The single-time relaxation scenario for such peak appears to be inadequate²⁶ because the relaxation induced change of the real part appears to be significantly larger than it should follow from the observed maximum of the imaginary part of the generalized response. This situation can be referred to as the puzzle

of "missing dissipation". In order to fix the problem on empirical level, various wide distributions of relaxation times can be invoked^{27,15}. As we have mentioned above, such conjectures, while providing a convenient empirical framework, do not explain the origin of the wide distribution in relatively good quality crystals.

Here we argue that, in addition to the dynamical variations of the real and imaginary parts of the response which are connected by the Kramers-Kronig relation, Peierls and ³He pinning potentials induce a purely equilibrium temperature-variation of the real part (at zero frequency ω)¹⁴ which is not directly linked to any dissipative process. This relaxes the "constraint" between the real and imaginary parts of G .

In order to illustrate the two origins of the shear modulus softening we introduce a linearized version of the model (1) which takes into account the pinning gap Δ : all the non-linear terms are replaced by $\sim K^{-1}\Delta^2 y^2/2$. The corresponding dynamical equation of the string biased by a small external stress $\sigma(t) \sim \exp(-i\omega t)$

$$\ddot{y}(x,t) - \nabla_x^2 y(x,t) + \int_0^\infty dt' \varepsilon(t') y(x,t-t') + \Delta^2 y(x,t) = \sigma(t), \quad (7)$$

with the boundary condition $y(x = \pm L/2, t) = 0$, in addition to the standard relaxation-dissipation term $\sim \varepsilon$ (see in Ref.¹⁶), includes the gap term $\sim \Delta^2$ induced by Peierls and ³He pinning. As shown above, Δ can be found from purely thermodynamical simulations of the full model (1) (see also in Ref.¹⁴).

The nature of the dissipative kernel $\varepsilon(t')$ at low T represents a separate fundamental problem. In this regard, we note the proposal²⁸ that dislocation kinks initiate strong dissipation in solid ⁴He²⁹. Similarly, the origin of the so called Bordoni peak in the internal friction in metals has also been assigned to kinks³⁰. Both approaches rely on the standard treatments in terms of the kinetic equation, without, however, addressing explicitly the issue of the integrability of the Sine-Gordon model (that is, that there should be no dissipation in it!).

Here we conjecture that the main source of the dissipation are the kink-kink collision processes described in Ref.³¹ under the assumption of the integrability broken by the spatial discretization of the Sine-Gordon description. Then, the long-time kink motion is described by diffusion coefficient $D \sim \exp(\Delta/T)/\Delta$, Ref.³¹. This corresponds to $\varepsilon(t') \sim \delta(t')/D = C_o \Delta \exp(-\Delta/T)$ in Eq.(7) (where $C_o \sim 1$ in chosen units), so that the space-dispersive relaxation is given by $\sim Dq^2$ with q standing for wave-vector along the dislocation. Such form implies that the dissipation vanishes as $T \rightarrow 0$, when the kink density $\sim \exp(-\Delta/T) \rightarrow 0$, and also as the gap $\Delta(T) \rightarrow 0$ at large T , when kinks overlap and loose their meaning.

Now we calculate the generalized shear modulus $G(\omega)$ in the frequency domain as $G^{-1} = G_{el}^{-1} + (\Lambda n_d/L) \int_0^L (y/\sigma) dx$ (see the explanation above Eq.(3)). Then solving Eq.(7) in Fourier with the zero-boundary condition we obtain

$$G^{-1}(T, \omega) = G_{el}^{-1} + \frac{\Lambda_0}{[\Omega(T, \omega)L/2]^2} \left(1 - \frac{\tanh[\Omega(T, \omega)L/2]}{\Omega(T, \omega)L/2} \right), \quad (8)$$

$$\Omega^2(T, \omega) \equiv -i\omega C_o \Delta e^{-\Delta/T} - \omega^2 + \Delta^2. \quad (9)$$

The constant $\Lambda_0 \equiv \Lambda n_d L^2$ (which is independent of L !) is determined by the total softening effect. Specifically, at $T = 0$ and $\omega = 0$, $\Omega \sim \mathcal{O}(1)$ and $G^{-1} - G_{el}^{-1} \sim$

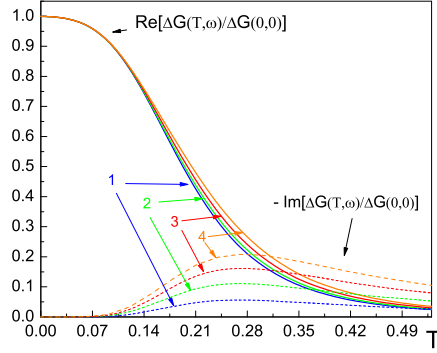


Fig. 4 (Color online) The real (solid lines) and imaginary (dashed lines) parts of the variation of the generalized shear modulus G given in Eqs.(8,9) normalized by the total variation of G from $T = 0$ to $T = \infty$. The family of four curves corresponds to four values of the dissipation strength C_o shown in the plot. The other chosen parameters are: $\Delta_1 = 0.1$, $\Delta_0 = 0.05$, $L = 100$, $\omega = 0.003$, $\Lambda_0 G_{el} = 0.4$ (in the dimensionless units discussed in the main text).

$1/L^2 \rightarrow 0$ for $L \gg 1$, and at $\omega = 0$ and large T when $\Delta = 0$: $G^{-1}(\infty, 0) - G_{el}^{-1} = \Lambda_0/12$.

A particular form of $\Delta(T)$ fitting well the experimental data was found to be $\Delta(T) = \Delta_1(1 - \exp(-\Delta_0/T))^2$, where Δ_0 depends on the strength of the Peierls and ^3He pinning potentials as well as on n and $\Delta_1 \sim 0.1$ is a constant. We have used these expressions in Eqs.(8,9) and have calculated the real and imaginary parts of the shear modulus, Fig. 4. As can be seen, in contrast to the simplistic single-relaxation-time model^{26,15}, the variations of the real and imaginary parts are not restricted by the condition that the maximum of the imaginary part is given by one-half of the total variation of the real part. Instead, while the real part is weakly dependent on the dissipation strength C_o and is mostly controlled by the T -dependence of the gap Δ , the imaginary part is strongly dependent on the value of the friction coefficient C_o , and, in principle, can be zero.

4 Kink-controlled core superfluidity

Here we will give details of the proposal¹¹ linking the shear modulus anomaly to the superfluid response. Its main ingredient is a strong interaction between the core superfluidity^{9,10} and density of kinks along the core. We will take into account this effect within the coarse grained mean field description relying on the bulk-averaged SF order parameter ψ as well as on the bulk-averaged density of kinks n_k . The interaction free energy between the two is taken in the minimal form $F_{\text{int}} = g_1 n_k |\psi|^2 > 0$, with $g_1 > 0$ being some phenomenological coefficient. Thus, the full bulk free energy density takes the form

$$F = a'(T - T_0)|\psi|^2 + \frac{g_2}{2}|\psi|^4 + g_1 n_k |\psi|^2 + \Delta(T) \cdot n_k + T n_k \ln(n_k/(n_0 e)), \quad (10)$$

where $a' > 0, g_2 > 0$ are the standard Landau-expansion coefficients with T_0 corresponding to the mean field SF-transition temperature. The term $\sim \Delta$ describes energy of thermal activation of kinks and the last one accounts for the entropy of the kink gas in the limit $n_k \ll n_0$, where n_0 stands for the maximum bulk concentration of kinks determined by the size of the Sine-Gordon soliton $\propto 1/\sqrt{\Delta}$ and the density of dislocations n_d . Here kinks are treated as Boltzmann particles.

We note that, formally, the model (10) apart from the kink-terms coincides with the approach³². However, in contrast to Ref.³² advocating a true supersolidity in ⁴He, we view the formation of the SF order parameter as being due to a network of dislocations with superfluid cores^{33,9,10}. In this analysis we don't consider that some dislocations exhibit superclimb and the anomalous compressibility¹⁰. The coarse grained description of such network is a separate interesting problem.

4.1 The Mean Field phase diagram

The equilibrium of the system can be determined from the minimization $\delta F/\delta\psi^* = 0$ and $\delta F/\delta n_k = 0$:

$$[a'(T - T_0) + g_1 n_k] \psi + g_2 |\psi|^2 \psi = 0, \quad n_k = n_0 \exp\left(-\frac{\Delta + g_1 |\psi|^2}{T}\right). \quad (11)$$

The first equation can be formally written as a relative value of the condensate density $\rho_s(T) = |\psi|^2$ as

$$\tilde{\rho}(T) = \frac{\rho_s(T)}{\rho_s(0)} = 1 - \frac{T}{T_0} - \frac{g_1 n_k}{g_2 \rho_s(0)}, \quad (12)$$

where $\rho_s(0) = a'T_0/g_2$ and we took into account that $n_k(T = 0) = 0$.

Eqs.(11) describe the mean field phase diagram featuring lines of II and I order transitions with the tricritical point separating them. It is convenient to introduce the following dimensionless quantities

$$C_1 = \frac{a'(T_0 - T)}{g_1 n_0} \exp\left(\frac{\Delta}{T}\right) > 0, \quad C_2 = \frac{g_2 T}{g_1^2 n_0} \exp\left(\frac{\Delta}{T}\right) > 0, \quad (13)$$

for $T < T_0$. Then, the II order (mean field) transition takes place along the line $C_1 = 1, C_2 > 1$. Along this line F has only one minimum $\psi = 0$ for $C_1 < 1$ and $\psi \neq 0$ for $C_1 > 1$, with $n_k \neq 0$ in both phases. As $C_2 < 1$, F can have two coexisting minima. That is, the I order transition occurs for $C_2 < 1$, with the tricritical point located at $C_1 = C_2 = 1$. The actual equation for the I order transition line (when both minima have equal free energies) cannot be solved explicitly. Its numerical solution is represented by thick red line in Fig. 5.

The boundaries (spinodals) within which F has two minima, that is, where metastable superfluidity can exist, can be found analytically. These are given by $C_2 < 1, C_s(C_2) < C_1 < 1$ where

$$C_s(C_2) = C_2 \ln\left(\frac{e}{C_2}\right), \quad 0 < C_2 \leq 1. \quad (14)$$

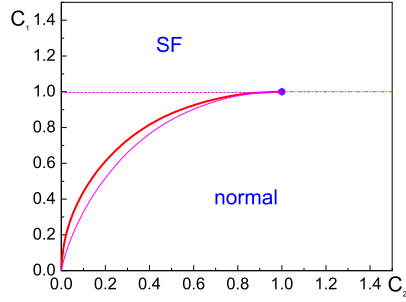


Fig. 5 (Color online) The mean field phase diagram of the model (11) in terms of the variables (13). Solid red and dashed dark yellow lines represent the I and II order phase transitions, respectively. The large blue dot denotes the tricritical point separating the II and I order transitions. The domains above and below the transition lines marked as SF and as "normal" correspond to the SF and the normal states, respectively. The thin pink curve indicates the spinodal $C_s(C_2)$, Eq.(14). The metastable superfluidity can occur above this line and below the pink dashed straight line $C_1 = 1, C_2 < 1$.

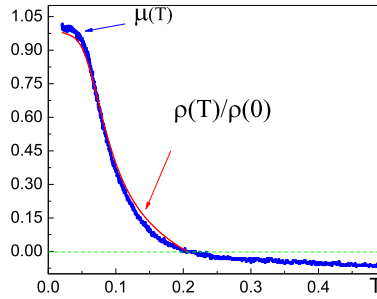


Fig. 6 (Color online) Blue dots: Relative shear modulus, Eq.(21), with $T_c = 0.21K$, from ⁴. Red line – relative superfluid density obtained from Eq.(12). Green dashed line shows zero for $\rho_s(T)$ at $T = T_c$.

4.2 Similarity between static superfluid and mechanical responses

Here we will discuss the striking similarity between the SF response $\rho_s(T)$ and $G(T)$ following from the model introduced above (cf. in Ref.⁴). It occurs along the II order line due to the strong interaction between kinks and superfluidity given by the term $\sim g_1$ in Eq.(10). Let's consider the system far from the tricritical point, $C_2 \gg 1$, and close to the II order line, $C_1 \approx 1$. The condition $C_1 = 1$ determines the mean field transition temperature T_c as

$$\exp\left(\frac{\Delta}{T_c}\right)(1 - T_c/T_0) = \frac{g_1 n_0}{a'T_0}. \quad (15)$$

If

$$\frac{g_1 n_0}{a' T_0} \gg 1, \quad (16)$$

which constitutes the condition of strong kink-superfluid interaction, one finds

$$T_c \approx \frac{\Delta}{\ln(g_1 n_0 / a' T_0)} \ll T_0. \quad (17)$$

At this point it is important to mention that the temperature T_c is rather a renormalized value of T_0 than the actual transition of establishing the 3D coherence. In other words, it is the *onset* temperature where the NCRI should appear in a sense of the Shevchenko state³³ (cf. the vortex-fluid model³⁴).

The condition that the system is far from the I order transition $C_2 \gg 1$ in combination with $T_c \ll T_0$, Eq.(16), gives

$$\frac{g T_c}{g_1 a' T_0} \gg 1. \quad (18)$$

To what extent this condition is satisfied in solid ⁴He remains to be seen.

Let us demonstrate the similarity between the mechanical and superfluid responses in the limit (16). In the limit (18) T should be dropped from the definition of C_1 in Eq.(13) for $0 < T < T_c$, so that the solution for the superfluid fraction $\rho_s(T) = |\psi|^2$, Eqs.(11), can be formally rewritten in the form

$$\frac{\rho_s(T)}{\rho_s(0)} = 1 - \frac{n_k(T)}{n_k(T_c)}, \quad T \leq T_c \quad (19)$$

where $n_k(T)$ obeys Eq.(11) and T_c is given in Eq.(17).

The shear modulus thermal softening discussed above in Sec.2 is determined by the averaged density of thermal kinks n_k . Indeed, Eq.(3) relates the $G(T)$ softening to the fluctuations of the string displacement $\langle y^2 \rangle$ which, in its turn, is determined by the density of thermal kinks n_k . Qualitatively, one finds $\langle y^2 \rangle \propto n_k$ at least at low T where kinks are still well defined entities. Thus, the shear modulus G given by Eq.(3) can be rewritten in terms of the coarse grained kink density as

$$G(T) = \frac{G_0}{1 + \tilde{A} n_k(T)}, \quad (20)$$

where $G_0 = G(T=0) \approx G_{el}$ and the prefactor \tilde{A} can be taken as a constant of T for all practical purposes because it does not contain any exponential.

We introduce the relative change of the shear modulus with respect to its value $G(T_c)$ at the transition temperature (where ρ_s is zero):

$$\mu(T) = \frac{G(T) - G(T_c)}{G(0) - G(T_c)}. \quad (21)$$

Substituting G from Eq.(20), we find

$$\mu(T) = \frac{1}{1 + \tilde{A} n_k(T)} \left(1 - \frac{n_k(T)}{n_k(T_c)} \right) \approx \frac{\rho_s(T)}{\rho_s(0)} \quad (22)$$

where the last line follows from Eq.(19) and the factor $1/(1 + \tilde{A}n(T)) \approx 1$ because it controls the total relative variation of the modulus within only 5-15%⁴. Thus, within such accuracy, our model naturally features the close similarity between the relative variations of the superfluid and mechanical responses.

It should, however, be mentioned that the above simplified model cannot be applied to temperatures significantly above the gap value $\Delta(T=0)$, that is, when the simple activation dependence $n_k \propto \exp(-\Delta/T)$ does not fit well (see in Ref.¹⁴) the actual experimental data Ref.⁴. Nevertheless, Eq.(12) does not actually rely on the simple activation form of the kink density and will remain the same regardless of a particular form of the kink free energy. Thus, the actual form of n_k at elevated T can be extracted from the experiment⁴ with the help of Eq.(20). Then, substituting the so found $n_k(T)$ into Eq.(12) and using g_1/a' as the only adjustable parameter for chosen $T_0 = 1K$, we find $T_c = 0.21K$ and obtain the graph Fig.6. It shows the data from Ref.⁴, $f = 2000\text{Hz}$, plotted together with the relative superfluid density $\tilde{\rho}_s(T)$ obtained from Eq.(12). The similarity between the two responses is obvious.

Concluding this section, we note that the energy Δ sets the scale for both— $G(T)$, below which it stiffens, and for the onset temperature T_c of the SF response. As discussed in Sec.2.1, adding ³He increases Δ and, therefore, increases the SF onset temperature.

4.3 Similarity between the dissipative responses.

The similarity between the SF and mechanical responses considered above is not limited to the static case. Obviously, a strong coupling $\sim g_1$ must induce the same dissipation in both subsystems. As a result, excitations in the SF network will show damping similar to the one introduced into Eq.(7). Such excitations lead to a dynamical mass (and the moment of inertia) redistribution inside the TO cell. Accordingly, the TO response should show the dissipation as long as SF currents percolate along a non-uniform network which, in general, allows linear coupling between SF phase and rotation. We demonstrate the similarity between the dissipation (in the shear modulus and in the SF excitations) in the mean field equations for small oscillations of the SF order parameter. Using the hydrodynamic approximation $\psi = \sqrt{\rho}e^{i\phi}$ for the conjugate variables ρ, ϕ in F , Eq.(10), and the canonical commutation relations, we find Hamiltonian equation for ρ from (10). For n_k as classical particles we use linearized kinetic equation (cf.²⁸) in the single-time τ relaxation approximation which ignores spatial dispersion: $\dot{n}_k = -\frac{1}{\tau}\delta F/\delta n_k$. This gives

$$\ddot{\rho} - \rho_0 \nabla^2 (g_2 \rho + g_1 n_k) = 0, \quad \dot{n}_k = -\frac{1}{\tau} (n_k - n^{(eq)}), \quad (23)$$

where ρ_0 denotes the coarse grained SF density; $n^{(eq)}$ stands for the quasi-equilibrium density of kinks given by Eq.(11). The small variation $\delta n^{(eq)}$ of $n^{(eq)}$ induced by the time dependent part ρ' of $\rho = \rho_0 + \rho'$ can be found from minimizing the free energy (10) in the linear approximation as:

$$\delta n^{(eq)} = -\frac{g_1 n_0^{(eq)}}{T} \rho', \quad n_0^{(eq)} = n_0 \exp\left(-\frac{\Delta + g_1 \rho_0}{T}\right) \quad (24)$$

where $n_0^{(eq)}$ stands for the static value of the kink density found from the second equation in (11). A substitution of $\delta n^{(eq)}$ into Eqs.(23) and further elimination of n_k in Fourier gives the dispersion relation for the SF excitations

$$-\omega^2 + c_0^2 q^2 \left[1 - \varepsilon'_0 \frac{i\omega\tau}{1 - i\omega\tau} \right] = 0, \quad \varepsilon'_0 \equiv \frac{g_1^2 n_0^{(eq)}}{T g_2}, \quad (25)$$

where q stands for the wave-vector and $c_0^2 = \rho_0(g_2 - g_1^2 n_0^{(eq)}/T)$ denotes speed of first sound.

The value of τ can be related to the relaxation in Eq.(7) as $\tau^{-1} \sim \varepsilon$. Thus, at $T \rightarrow 0$, where $\tau \sim \exp(\Delta/T) \rightarrow \infty$, and at $T \rightarrow \infty$, where $\tau \sim 1/\Delta(T) \rightarrow \infty$, the dissipation in Eq.(25) vanishes along with the dissipation of the shear modulus.

5 Discussion and perspectives

We have introduced the alternative to the traditionally accepted "boiling off" model of pinning gliding dislocations by ^3He impurities: Quantum and thermal fluctuations of dislocation shape lead to decoupling of dislocations from the Peierls and ^3He -pinning potentials at temperatures determined by the energy of kink-antikink pair.

The analysis of the shape of the shear modulus vs temperature at significantly different ^3He concentrations, Ref.⁴, and its comparison with the results of Monte Carlo simulations strongly indicate that the relaxation time for establishing equilibrium between ^3He impurities bound to dislocations and those which are free in the bulk is very large on any experimental time scale. This conjecture is supported by the estimates of the values of the trapping potential for ^3He and is consistent with the general nature of the narrow-band impuriton¹⁹. The formation of the two subsystems of ^3He atoms—free in the bulk and bound to dislocations—is most likely to occur during ^4He crystal growth. We find this problem as very important for theoretical and experimental studies.

It is shown that the shear modulus softening consists of two contributions: first, from thermally suppressed gap and, second, from dissipation. In general, these two effects are independent from each other so that the puzzle of "missing dissipation" can be resolved without invoking a wide distribution of relaxation times in relatively good quality crystals.

The minimal model leading to the similarity between the TO NCRI response and the generalized shear modulus has been developed. It is shown that the strong suppression of the superfluidity along dislocation core by dislocation kinks locks in both responses. In light of the recent work⁷ we note that the data which are well above the red line in Fig.1, Ref.⁷, does not exclude the genuine NCRI anomaly whose similarity to the mechanical response is determined by the mechanism described above.

The dissipation similarly seen in the TO and the shear modulus measurements is proposed to be attributed to the bath of dislocation kinks living along the dislocation network. The nature of such dissipation (its frequency and temperature dependencies) is linked to the fundamental question of how dissipation emerges in a network of 1d systems and, therefore, deserves close attention. Of a specific

interest is studying the dissipation in the system of superclimbing dislocations, where the spectrum is not sound-like anymore¹⁰.

Another interesting aspect is how the SF fraction and its excitations can be detected in the UMass-Sandwich-type setup⁸. Currently, the detected flow is d.c. and is in the overcritical (strongly non-linear) regime and, therefore, is not suitable for answering these questions. Thus, it is important to devise and implement the a.c. current sandwich-type setup in order to study the linear response of the SF network directly.

Acknowledgements We are grateful to John Beamish for providing the experimental data and useful discussions. We also thank Nikolay Prokof'ev and Boris Svistunov for many stimulating discussions. This work was supported by the National Science Foundation under Grant No.PHY1005527, and by a grant of computer time from the CUNY HPCC under NSF Grants CNS-0855217 and CNS - 0958379.

References

1. E. Kim and M.H.W. Chan, *Nature* **427**, 225 (2004); E. Kim and M.H.W. Chan, *Science* **305**, 1941 (2004).
2. A. J. Leggett, *Phys. Rev. Lett.* **25**, 1543 (1970).
3. E. P. Gross, *Phys. Rev.* **106**, 161 (1957); E. P. Gross, *Annals of Physics* **4**, 57(1958); A. F. Andreev and I. M. Lifshitz, *Sov. Phys. JETP* **29**, 1107 (1969); D. J. Thouless *Ann. Phys.* **52**, 403(1969) G. V. Chester, *Phys. Rev. A* **2**, 256 (1970).
4. J. Day and J. Beamish, *Nature* **450**, 853 (2007); J. Day, O. Syshchenko, and J. Beamish, *Phys. Rev. B* **79**, 214524(2009).
5. V.L. Tsymbalenko, *Sov. Phys. JETP* **60**, 537(1984).
6. J. Reppy, *Phys. Rev. Lett.* **104**, 255301 (2010); X. Mi, E. Mueller, J. D. Reppy, arXiv:1109.6818.
7. J. R. Beamish, A. D. Fefferman, A. Haziot, X. Rojas, and S. Balibar, *Phys. Rev. B* **85**, 180501(R) (2012).
8. M. W. Ray and R. B. Hallock, *Phys. Rev. Lett.* **100**, 235301 (2008); *Phys. Rev. B* **79**, 224302 (2009).
9. M. Boninsegni, A. B. Kuklov, L. Pollet, N. V. Prokof'ev, B. V. Svistunov, and M. Troyer, *Phys. Rev. Lett.* **99**, 035301 (2007).
10. Ş. G. Söyler, A. B. Kuklov, L. Pollet, N. V. Prokof'ev, and B. V. Svistunov, *Phys. Rev. Lett.* **103**, 175301 (2009).
11. D. Aleinikava, E. Dedits, A. B. Kuklov, D. Schmeltzer, arXiv:0812.0983 .
12. S. Balibar, *Physics* **3**, 39 (2010): <http://physics.aps.org/articles/v3/39>; *Nature* **464**, 176 (2010).
13. J. Friedel, *Dislocations*, Pergamon Press, 1964.
14. D. Aleinikava, E. Dedits, A. B. Kuklov, and D. Schmeltzer, *Europhys. Lett.*, **89**, 46002 (2010).
15. O. Syshchenko, J. Day, and J. Beamish, *Phys. Rev. Lett.* **104**, 195301 (2010).
16. A. Granato and K. Lücker, *J. Appl. Phys.* **27**, 583 (1956); *ibid.* 789(1956).
17. P. Corboz, L. Pollet, N. V. Prokof'ev, and M. Troyer *Phys. Rev. Lett.* **101**, 155302 (2008).

-
18. C. Zhou, J.-J. Su, M. J. Graf, C. Reichhardt, A.V. Balatsky, I. J. Beyerlein, arXiv: 1110.0841.
 19. A.F. Andreev, Sov. Phys. Usp. **19**, 137(1976).
 20. N.V. Prokof'ev and B.V. Svistunov, Phys. Rev. Lett. **87**, 160601 (2001).
 21. D. Aleinikava and A.B. Kuklov, arXiv:1108.1182,
 22. A good fit can only be achieved for the very unrealistic values: $n_d \sim 10^{-2}$, $X_3 \sim 10^{-2}$, $E_a = 0.2 - 0.3K$.
 23. Yu. Kagan and L.A. Maksimov, Sov. Phys. JETP **38**, 307(1974).
 24. I. Iwasa, H. Suzuki, J. Phys. Soc. Japan, **49**, 1722(1980).
 25. M. A. Paalanen, D. J. Bishop, and H. W. Dail, Phys. Rev. Lett. **46**, 664 (1981).
 26. C.-D. Yoo and A. T. Dorsey, Phys. Rev. **B 79**, 100504(R) (2009).
 27. Z. Nussinov, A. V. Balatsky, M. J. Graf, and S. A. Trugman, Phys. Rev. **B 76**, 014530 (2007).
 28. A.V. Markelov, Sov. Phys. JETP **61**, 118(1985).
 29. Y. Hiki and F. Tsuruoka, Phys. Lett. **A 62**, 50(1977); F. Tsuruoka and Y. Hiki, Phys. Rev. **B 20**, 2702(1979); V. L. Tsybalenko, Sov. Phys. JETP **47**, 1507 (1978).
 30. F. Marchesoni, Phys. Rev. Lett. **74**, 2973(1995).
 31. K. Damle and S. Sachdev, Phys.Rev.Lett. **95**, 187201 (2005).
 32. P.W. Anderson, Science **324**, 631 (2009);
 33. S. I. Shevchenko, Sov. J. Low Temp. Phys. **13**, 61 (1987); D. V. Fil and S. I. Shevchenko, Phys. Rev. **B 80**, 100501 (2009).
 34. P. W. Anderson, Nature Physics **3**, 160 (2007)